IEEE Access
Multidisciplinary | Rapid Review | Open Access Journal

Received October 9, 2019, accepted October 17, 2019, date of publication October 22, 2019, date of current version November 1, 2019.

Digital Object Identifier 10.1109/ACCESS.2019.2948843

Design, Modeling and Synthesis of Negative Group Delay IL-Shape Topology

BLAISE RAVELO, (Member, IEEE), NINGDONG LI, FAYU WAN, (Member, IEEE), AND JIAO FENG

Nanjing University of Information Science and Technology (NUIST), Nanjing 210044, China

Corresponding author: Jiao Feng (jiao.feng@nuist.edu.cn)

This work was supported in part by the NSFC under Grant 61971230 and Grant 61601233, in part by the Jiangsu Distinguished Professor program and Six Major Talents Summit of Jiangsu Province under Grant 2019-DZXX-022, in part by the Postgraduate Research and Practice Innovation Program of Jiangsu Province under Grant SJKY19_0974, and in part by the Priority Academic Program Development of Jiangsu Higher Education Institutions (PAPD) fund.

ABSTRACT This paper introduces a negative group delay (NGD) theory of passive topology presenting "IL"-shape geometry. The two-port topology is comprised of a coupled line with an open- and stub-loaded terminations. After introduction of the electrical equivalent circuit, the S-parameter modeling of the IL topology is established. The transmission and reflection parameters are analytically expressed. The IL topology NGD characterization is developed in function of the design parameters. The relevance of the NGD theory is verified with fully distributed and compact prototypes implemented in microstrip technology. The tested results confirm the possibility to generate bandpass NGD function with IL topology. The calculated model, simulation and measurements are in very good correlation. Validation results showing center frequencies at about 1.55 GHz and 3.55 GHz with NGD level better than −1 ns over 30 MHz bandwidth. The IL NGD prototypes present transmission and reflection coefficients better than −3 dB and −10 dB, respectively.

INDEX TERMS Microwave circuit theory, IL-shape topology, distributed topology, negative group delay (NGD), coupled lines, S-matrix modeling.

I. INTRODUCTION

Behind the spectacular progress of radio frequency and microwave communication systems, the delay effects seem as an insurmountable performance limiting factor [1]–[4]. In addition to the noise, the group delay (GD) limits the performances of wireless communication functions [2] as filters [1]. In addition to the GDs, the electrical interconnect propagation delay which can be represented by RC-networks degrades the communication signal integrity [3], [4].

Despite this undesirable limitation, an attempt to design delay insensitive circuits was proposed [5]. Delay line-based RF, microwave and optical circuits were also proposed [6]–[9]. A methodology to design recirculating delay line systems was introduced [6]. Beamforming fan filters using time delay approximations were developed [7]. A design method of channel blind identification based on the GD was also proposed [8]. In optical wavelengths, optical delay-based filter was introduced [9]. An intriguing way to reduce GD with negative refractive index (NRI) transmission line (TL) was initiated in [10]. This counterintuitive NRI aspect was approved by the observations as the negative GD (NGD) in a photonic crystal structure [11].

The NGD state of the art starts with the Brillouin theoretical investigation on the dispersive and absorptive optical media [12]. It was shown that the NGD phenomenon can be occurred around the resonance frequency of the absorptive media presenting frequency dependent refractive index $n(\omega)$ in function of the angular frequency ω. In a such absorptive media, the group velocity can be expressed as:

$$v_g(\omega) = \frac{c}{\Re e\left[n(\omega) + \omega\dfrac{\partial n(\omega)}{\partial \omega}\right]}, \tag{1}$$

with c is the vacuum light speed. Obviously, quantity v_g can be negative when the following condition is

The associate editor coordinating the review of this manuscript and approving it for publication was Yilun Shang.

correctly satisfied:

$$\frac{\partial n(\omega)}{\partial \omega} < 0. \tag{2}$$

Therefore, through the media presenting physical length d, the group delay:

$$\tau(\omega) = \frac{d}{v_g(\omega)}, \tag{3}$$

may become negative if $v_g < 0$. The meaning of the NGD in the time-domain was firstly explained in [13]. The NGD phenomenon was illustrated by propagating a Gaussian light pulse through an anomalous dispersion medium. Afterwards, the NGD first experimental investigations were performed [14], [15].

The first microwave NGD circuits were synthesized in 1990s [16], [17]. The NGD lumped passive circuits were established from the periodical NRI TLs in parallel with the deployment of metamaterial concept [18]–[20]. Synthesis methods of R, L and C component based NGD circuits were developed [21], [22]. The NGD concept understanding leads to the certain NGD application propositions [23]–[32] notably in the field of RF and microwave engineering. A microwave GD time adjuster was proposed in [23], [24]. A GD equalized ultra-wide band amplifier using NGD circuits was introduced in [25]. A design method of feedforward amplifier for the bandwidth enhancement was presented in [26]. The NGD was also used to realize a bilateral gain-compensated circuit [27]. By cascading with a TL, the NGD function enabled to synthesize a frequency independent phase shifter [28]. More intriguingly, the NGD circuits were implemented to realize non-Foster reactive elements [29], [30] which were used to design an arbitrary-angle squint-free beamforming in series-fed antenna arrays [31]. The NGD function was more recently used to design a tunable delay shifter [32]. A bi-directional amplifier using NGD matched circuits was designed in [33]. Despite this progressive development of NGD applications, further efforts have to be conducted to overcome the limitations in terms of losses [18]–[20], operation frequency bandwidth, design complexity and the implicit asymptotic limits of active circuits [34].

To overcome these limitations, research works have been conducted to design different topologies of distributed NGD networks [35]–[38]. One of simplest distributed NGD proposal is based on the use of two parallel lines [35]–[38]. A design method of NGD microwave circuits based on the signal interference technique is introduced in [35]. An analysis of three parallel line NGD structure is proposed in [36]. A transmission type NGD structure is developed in [37]. A feedback delayed coupler based coupled lines is introduced in [38]. But all these NGD circuits operate with rather complex topology. We are constantly wondering about the NGD function design feasibility of simpler topology. For this reason, we intuitively think on the direct transmission of coupled line topology.

This innovative idea is deeply investigated in the present paper by considering the distributed topology of ''IL''-shape geometry structure. The circuit is assumed as a two-port topology. The paper is organized in four main sections as follows:

- Section II is focused on the topological description and the general S-matrix modeling.
- Section III develops the innovative NGD theory of IL-shape geometry structure. After the GD expression, the NGD analysis is introduced with the NGD condition in function of the IL topology parameters. The GD formulation at particular frequencies are expressed and analyzed.
- Hence, Section IV focuses on the validation results. After the proof-of-concept description, the simulated and experimented results will be discussed. Comparisons of simulated and measured GDs will be performed.

Lastly, Section V is the conclusion of the paper.

II. S-MATRIX ANALYTICAL MODELLING OF THE PROPOSED IL-SHAPE TOPOLOGY

The analytical investigation is developed in this section. First and foremost, the IL shape topology is defined and electrically described. The equivalent diagram illustrating the analytical interaction between the elementary constituting elements of the basic topology is presented. The analytical modeling is established from the S-matrix operation.

A. DESCRIPTION OF THE IL-SHAPE TOPOLOGY

Fig. 1 depicts and illustrates the configuration of the IL shape structure topology under study. This interesting topology fully constituted by distributed elements does not use any lossy lumped and even a single resistor. It acts as a two-port circuit denoted by reference plans ① and ②. The IL topology is comprised of:

- Parallel coupled line CL(ζ,R_0) with coupling coefficient ζ and characteristic impedance R_0 which is also the reference impedance of the S-parameters. The CL is a four-port component which is referenced by internal ports ❶, ❷, ❸ and ❹.
- And the stub TL(R_0, a, τ_s) with characteristic impedance R_0, attenuation loss a and delay τ_s. The stub is terminated by the impedance Z_L which enables to

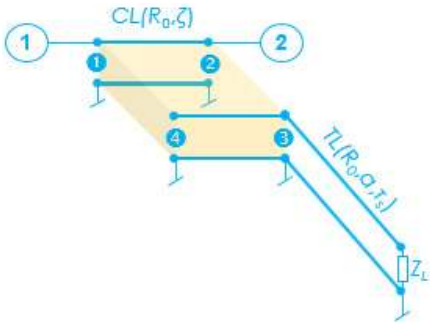

FIGURE 1. IL topology configuration.

generalize the two cases of open- ($Z_L = \infty$) and short- ($Z_L = 0$) circuit terminations to be developed in the remainder part of this paper.

The associated S-matrix will be explored in the next subsection.

B. IL TOPOLOGY S-MATRIX

The IL topology S-matrix is established by means of the equivalent diagram introduced in Fig. 2. This diagram consists of the coupled line black box and the stub TL input impedance Z.

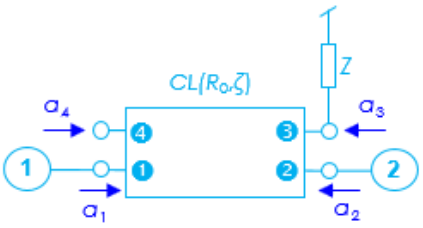

FIGURE 2. IL topology equivalent diagram.

1) RECALL ON COUPLED LINE S-MATRIX AND STUB INPUT IMPEDANCE

According to the microwave theory, the coupled line S-parameter model can be written as [12]:

$$[S_{CL}] = \begin{bmatrix} 0 & \varpi & 0 & \zeta \\ \varpi & 0 & \zeta & 0 \\ 0 & \zeta & 0 & \varpi \\ \zeta & 0 & \varpi & 0 \end{bmatrix}, \tag{4}$$

by denoting the angular frequency variable ω and the complex number $j = \sqrt{-1}$ with:

$$\begin{cases} \zeta_0 = \sqrt{1-\zeta^2} \\ \varpi = -j\zeta_0. \end{cases} \tag{5}$$

By taking:

$$x = e^{-j\omega\tau_s}, \tag{6}$$

the open-ended and short-circuited stub input impedance is defined by:

$$Z = \begin{cases} R_0 \dfrac{1+a^2x^2}{1-a^2x^2} & if\ Z_L = \infty \\ R_0 \dfrac{1-a^2x^2}{1+a^2x^2} & if\ Z_L = 0. \end{cases} \tag{7}$$

2) S-MATRIX MODELLING METHODOLOGY

Identified as a two-port passive topology, the frequency-dependent S-matrix of the IL topology is traditionally written as:

$$[S(j\omega)] = \begin{bmatrix} S_{11}(j\omega) & S_{21}(j\omega) \\ S_{21}(j\omega) & S_{22}(j\omega) \end{bmatrix}. \tag{8}$$

By considering the wave power definition, the S-matrix can be linked to input and output wave power vectors $\begin{bmatrix} a_1 \\ a_2 \end{bmatrix}$ and $\begin{bmatrix} b_1 \\ b_2 \end{bmatrix}$, respectively by the relation:

$$\begin{bmatrix} b_1 \\ b_2 \end{bmatrix} = [S] \times \begin{bmatrix} a_1 \\ a_2 \end{bmatrix}. \tag{9}$$

For more rigorous approach, the IL topology can be theoretically modelled with the analytical approach including the traditional input and output wave powers a_m and $b_m (m = \{1, 2, 3, 4\})$ from the coupled line access ports:

$$\begin{bmatrix} b_1 \\ b_2 \\ b_3 \\ b_4 \end{bmatrix} = [S_{CL}] \times \begin{bmatrix} a_1 \\ a_2 \\ a_3 \\ a_4 \end{bmatrix}. \tag{10}$$

The S-matrix of expression (9) can be determined from matrix relation (10) by eliminating $a_{3,4}$ and $b_{3,4}$. As port ❸ is loaded by the shunt impedance Z, the associated reflection coefficient is equal to:

$$\frac{a_3}{b_3} = \frac{Z - R_0}{Z + R_0}. \tag{11}$$

This relationship can also be transformed as:

$$a_3 = \frac{Z - R_0}{Z + R_0} b_3. \tag{12}$$

As port ❹ is open-ended, the input and output wave powers must be identical:

$$b_4 = a_4. \tag{13}$$

Following the configuration of the circuit explicated in Fig. 2, S_{11}, S_{21} and S_{22} can be analytically determined by the reduction of matrix (10). After algebraic calculations, we obtain the following general expressions:

$$S_{11} = \frac{\zeta^2(Z + R_0)}{\zeta^2 R_0 + (2 - \zeta^2)Z} \tag{14}$$

$$S_{22} = \frac{\zeta^2(Z - R_0)}{\zeta^2 R_0 + (2 - \zeta^2)Z} \tag{15}$$

$$S_{21} = \frac{-2j\zeta_0 Z}{\zeta^2 R_0 + (2 - \zeta^2)Z}. \tag{16}$$

C. S-MATRICES OF OPEN- AND SHORT-TERMINATED STUB IL TOPOLOGIES

As aforementioned, the NGD theory of the proposed IL topology is focused on two-simple cases of open- and short-circuit load Z_L. The S-matrix elements of the open-ended stub topology is written as:

$$S_{11_{open}} = \frac{\zeta^2}{1 + (a\,x\,\zeta_0)^2} \tag{17}$$

$$S_{21_{open}} = \frac{j\zeta_0(1 + a^2\,x^2)}{1 + (a\,x\,\zeta_0)^2} \tag{18}$$

$$S_{22_{open}} = \frac{(a\,x\,\zeta)^2}{1 + (a\,x\,\zeta_0)^2}. \tag{19}$$

The S-matrix of the short-circuit ended stub topology is written as:

$$S_{11_{short}} = \frac{\zeta^2}{1-(a\,x\,\zeta_0)^2} \tag{20}$$

$$S_{21_{short}} = \frac{j\zeta_0(1-a^2\,x^2)}{1-(a\,x\,\zeta_0)^2} \tag{21}$$

$$S_{22_{short}} = \frac{-(a\,x\,\zeta)^2}{1-(a\,x\,\zeta_0)^2}. \tag{22}$$

By reason of design simplicity, the next part of the study will be focused on the open-ended stub IL topology

III. NGD ANALYSIS OF OPEN-ENDED STUB BASED IL TOPOLOGY

This section introduces the IL topology NGD theory built with from the transmission coefficient. The NGD analysis is elaborated in function of the IL topology parameters.

A. FREQUENCY-DEPENDENT S-MATRIX OF THE IL TOPOLOGY

The frequency-dependent reflection and transmission coefficients can be derived from previous S-matrix operation. The analytical results are written as, respectively:

$$S_{11}(j\omega) = \frac{\zeta^2 e^{2j\omega\tau_s}}{a^2\zeta_0^2 + e^{2j\omega\tau_s}} \tag{23}$$

$$S_{21}(j\omega) = \frac{-j\zeta_0(a^2 + e^{2j\omega\tau_s})}{a^2\zeta_0^2 + e^{2j\omega\tau_s}} \tag{24}$$

$$S_{22}(j\omega) = \frac{\zeta^2 e^{2j\omega\tau_s}}{a^2\zeta_0^2 + e^{2j\omega\tau_s}}. \tag{25}$$

Acting as a fully distributed topology, the S-parameters are periodic expressions with angular frequency period:

$$\omega_p = 2\pi f_p = \frac{\pi}{\tau_s}. \tag{26}$$

The associated magnitudes are given by:

$$S_{11}(\omega) = |S_{11}(j\omega)| = \frac{\zeta^2}{\sqrt{1+a^4\zeta_0^4+2a^2\zeta_0^2\cos(2\omega\tau_2)}} \tag{27}$$

$$S_{21}(\omega) = |S_{21}(j\omega)| = \frac{\sqrt{1+a^2-2a^2\cos(2\omega\tau_2)}}{\sqrt{1+a^4\zeta_0^4+2a^2\zeta_0^2\cos(2\omega\tau_2)}} \tag{28}$$

$$S_{22}(\omega) = |S_{22}(j\omega)| = \frac{a^2\,\zeta^2}{\sqrt{1+a^4\zeta_0^4+2a^2\zeta_0^2\cos(2\omega\tau_2)}}. \tag{29}$$

Moreover, the transmission phase is expressed as:

$$\varphi(\omega) = \frac{\pi}{2} + \arctan\left[\frac{a^2-\cos(2\omega\tau_s)}{\sin(2\omega\tau_s)}\right] - \arctan\left[\frac{\sin(2\omega\tau_s)}{\cos(2\omega\tau_s)-\zeta_0^2a^2}\right]. \tag{30}$$

B. GD FREQUENCY-DEPENDENT EXPRESSION

By definition, the GD of the IL shape topology can be obtained from the transmission phase from the relation:

$$\tau(\omega) = -\frac{\partial\varphi(\omega)}{\partial\omega}. \tag{31}$$

For the sake of the mathematical simplification, this GD can be expressed as:

$$\tau(\omega) = \tau_b(\omega) - \tau_a(\omega) \tag{32}$$

with:

$$\tau_a(\omega) = \tau_s\left[1+\frac{1-a^4}{1+a^4+2a^2\cos(2\omega\tau_s)}\right] \tag{33}$$

$$\tau_b(\omega) = \frac{\tau_s\left[2-(2+a^2\zeta^2)\cos(2\omega\tau_s)\right]}{1+a^4\zeta_0^4-2a^2\zeta_0^2\cos(2\omega\tau_s)}. \tag{34}$$

Equation (32) explains that the IL topology GD depends on the coupled line coupling coefficient, attenuation a and linearly to the stub delay τ_s. In the next paragraphs of the present theoretical investigation, the NGD analysis will be theoretically performed by characterizing the NGD bandpass behavior of the IL topology. The analysis is concretely based on the functions GD and S_{21}.

C. NGD EXISTENCE CONDITION

First of all, the NGD existence analysis aims to prove following condition in function of the IL topology parameters:

$$\tau(\omega) < 0. \tag{35}$$

To do this, we can determine the frequency bands where condition (35) is undeniably satisfied. The mathematical analysis of the GD expressed in (31) enables to formulate the NGD existence condition in function of the IL topology parameters:

$$\psi(\omega) = \frac{n_1\cos(2\omega\tau_s)+n_0}{d_2\cos^2(2\omega\tau_s)+d_1\cos(2\omega\tau_s)-d_0} < 0 \tag{36}$$

with:

$$\begin{cases} n_1 = 1-a^4\zeta_0^2 \\ n_0 = 2a^2(\zeta^2-2) \\ d_2 = 4a^4\zeta_0^2 \\ d_1 = 2a^2(2-\zeta^2)(1-a^4\zeta_0^2) \\ d_0 = (1+a^4)(1+a^4\zeta_0^4). \end{cases} \tag{37}$$

1) GD NUMERATOR SIGN

We can remark that the numerator of quantity $\psi(\omega)$ is negative under condition:

$$\cos(2\omega\tau_s) < \frac{2a^2(2-\zeta^2)}{1-a^4\zeta_0^2}. \tag{38}$$

In other word, this condition is always satisfied when:

$$\frac{2a^2(2-\zeta^2)}{1-a^4\zeta_0^2} \geq 1. \tag{39}$$

The mathematical handling of this inequality enables to write:

$$\Rightarrow \zeta^2 \leq \frac{a^4+4a^2-1}{2a^2+a^4} = \frac{(a^2-1-\sqrt{5})}{a^2(2+a^2)}(a^2-1+\sqrt{5}). \quad (40)$$

If $a \leq 1/\sqrt{2}$, condition (38) is always satisfied. However, if $a > 1/\sqrt{2}$, the coupled line coupling coefficient must verify:

$$\zeta \leq \frac{\sqrt{a^4+4a^2-1}}{a\sqrt{2+a^2}}. \quad (41)$$

In this case, (34) can be rewritten as:

$$\frac{\arccos\left[\frac{2a^2(2-\zeta^2)}{1-a^4\zeta_0^2}\right]}{2\tau_s} < \omega < \frac{2\pi - \arccos\left[\frac{2a^2(2-\zeta^2)}{1-a^4\zeta_0^2}\right]}{2\tau_s}. \quad (42)$$

2) GD DENOMINATOR SIGN

The sign of the $\psi(\omega)$ denominator depends on the discriminant:

$$\Delta_\tau = d_1^2 - 4d_2d_0 = 4a^4\zeta^4(1-a^4\zeta_0^2)^2. \quad (43)$$

This discriminant is always positive whatever the coupling and attenuation loss. It means that inequality (32) can be verified when the angular frequency belongs to the interval:

$$\cos(2\omega\tau_s) < \frac{1-a^4\zeta_0^4}{2a^2(1-\zeta^2)}. \quad (44)$$

With the reciprocal representation, this inequality becomes implicitly:

$$\frac{\arccos\left[\frac{1-a^4\zeta_0^4}{2a^2(1-\zeta^2)}\right]}{2\tau_s} < \omega < \frac{2\pi - \arccos\left[\frac{1-a^4\zeta_0^4}{2a^2(1-\zeta^2)}\right]}{2\tau_s}. \quad (45)$$

D. NGD SPECIFIC FREQUENCIES

Acting as linear passive circuit, the spectrum of GD and the transmission coefficient magnitude $|S_{21}(j\omega)|$ or $|S_{21}(j\omega)|^2$ must present a similar behavior. Meanwhile, the two quantities must reach their optimal angular frequencies $\omega = \omega_o$. For the transmission coefficient, the minimal value can be expressed as:

$$S_{21}^2(\omega=\omega_o) = S_{21_{\min}}^2. \quad (46)$$

At the same frequency, the associated GD must also be minimal:

$$\tau(\omega=\omega_o) = \tau_{\min}. \quad (47)$$

When the transmission coefficient established in expression (28) reaches its minimal value, the reflection coefficient must complementarily reach its maximum:

$$S_{11}^2(\omega=\omega_o) = S_{11_{\max}}^2 \Rightarrow \left|1+a^4\zeta_0^4+2a^2\zeta_0^2\cos(2\omega\tau_c)\right|_{\min}. \quad (48)$$

It yields for $m = \{1, 2, 3, \ldots\}$, the optimal angular frequency from expression (23) when:

$$\cos(2\omega_o\tau_s) = -1. \quad (49)$$

The trigonometrical solution can be formulated as:

$$\omega_o(m) = \frac{m\pi}{\tau_s}. \quad (50)$$

In this case, the reflection and transmission coefficients introduced in (27), (28) and (29) become respectively:

$$S_{11}(\omega_o) = \frac{\zeta^2}{\sqrt{1-a^2\zeta_0^2}}, \quad (51)$$

$$S_{21}(\omega_o) = \frac{(1-a^2)\zeta_0}{\sqrt{1-a^2\zeta_0^2}}, \quad (52)$$

$$S_{22}(\omega_o) = \frac{a^2\zeta^2}{\sqrt{1-a^2\zeta_0^2}}. \quad (53)$$

Thus, the GD expressed in (31) is simplified as:

$$\tau(\omega_o) = \frac{-2a^2\zeta^2}{\zeta_0^2(1+a^2\zeta_0^2)}\tau_s. \quad (54)$$

We can emphasize that this GD is unconditionally negative. This last expression explains also the possibility to vary the NGD depth in function of the constituting coupled line length and coupling coefficient.

E. NGD FoM

The NGD topology performance depends mainly on:

- the NGD bandwidth $\Delta\omega$;
- the GD $\tau_o = \tau(\omega_o)$ at the NGD center frequency ω_o,

and secondarily to:

- the transmission coefficient $S_{21}(\omega_o)$;
- the reflection coefficient $S_{11}(\omega_o)$.

Accordingly, we reformulate the following equation to quantify this performance:

$$FoM_{NGD} = \Delta\omega \cdot \tau(\omega_o) \cdot \sqrt{\frac{S_{21}(\omega_o)}{S_{11}(\omega_o)}}, \quad (55)$$

F. NGD DESIGN PROCESS

The general process to design the NGD IL topology based circuit can be summarized with the seven steps as follows:

- ***Step 1***: Define the desired specifications:
  - NGD $\tau_o = \tau(\omega_o)$ value,
  - NGD center frequency ω_o,
  - Insertion loss $S_{21}(\omega_o)$,
  - Reflection loss $S_{11}(\omega_o)$,
- ***Step 2***: Determination of ideal IL cell parameters as the delay τ_s, coupling coefficient ζ and attenuation a,
- ***Step 3***: Ideal circuit simulations,
- ***Step 4***: Then, the NGD engineer must take care on the available technology for fabricating the NGD prototype.

- ***Step 5***: Then, realistic NGD circuit can be designed with the commercial tools (as in the present study, we will utilize with the RF and microwave circuit ADS® designer and simulator from Keysight Technologies®).
- ***Step 6***: In certain cases, optimizations are necessary to improve the NGD FoM by taking into account to the extra interconnect lines as the input/output access lines, the electrical interconnects and also the substrate material parameters provided by the manufacturer.
- ***Step 7***: In this last step, the NGD prototype can be fabricated from the circuit layout drawn from the optimized design performed in Step 6.

To verify the relevance of the IL NGD topology, simulation and experimental validations are discussed in the next section.

IV. SIMULATIONS AND EXPERIMENTAL VALIDATIONS OF THE IL NGD TOPOLOGY

The practical NGD validation of the IL shape NGD topology was carried out with two POCs. The proposed prototypes were designed, simulated, fabricated and tested. The simulations were carried out with the ADS® RF/microwave circuit designer and simulator software from Keysight Technologies®. Then, the frequency dependent GD and S-parameters from theoretical calculations, simulations and experimentations will be discussed in the next subsections.

A. DESCRIPTION OF IL NGD POC

Figs. 3 view the photographs of the prototypes of IL NGD POC with small (“S”) and large (“L”) physical sizes. Fig. 3(a) (resp. Fig. 3(b)) displays the S- (resp. “L”) IL prototype. These two-port prototypes are passive distributed circuits without lossy passive components even a resistor. They are implemented in microstrip technology. The microstrip circuits are printed on an FR4-epoxy substrate with Copper (Cu) metallization. The S- (resp. L-) IL ideal circuits was initially designed to operate at 3.58 GHz (resp. 1.555 GHz). Then, their geometrical parameters were slightly optimized with ADS® in order to take into account parasitic realistic effects of the metallization and the dielectric substrate. The final physical parameters of the constituting elements of each fabricated IL prototype are addressed in Table 1.

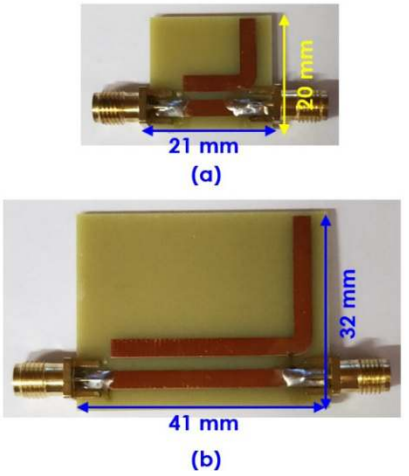

FIGURE 3. Photographs of fabricated (a) small (“S”) and (b) large (“L”) size IL shape NGD prototypes.

TABLE 1. IL prototypes’ parameters.

Components		*Description*	*Parameter*	*Value*
Dielectric substrate		Material	FR4-epoxy	-
		Relative permittivity	ε_r	4.4
		Loss tangent	tan(δ)	0.02
		Thickness	h	1.6 mm
Metallization		Material	Copper (Cu)	-
		Thickness	t	35 µm
		Conductivity	σ	58 MS/m
Stub line TL	“S”-IL	Physical length	d	12.35 mm
		Width	w	3 mm
		Attenuation loss	a	-0.22 dB
		Delay	τ_s	0.1 ns
	“L”-IL	Physical length	d	22.35 mm
		Width	w	3 mm
		Attenuation loss	a	-0.12 dB
		Delay	τ_s	0.16 ns
Coupled CL	“S”-IL	Width	w	3 mm
		Length	d_c	10 mm
		Interspace	s	1.4 mm
		Coupling coefficient	ζ	-16.64 dB
	“L”-IL	Width	w	3 mm
		Length	d_c	30 mm
		Interspace	s	2.2 mm
		Coupling coefficient	ζ	-20.4 dB
Access lines		Width	w	3 mm
		Physical length	d_a	6 mm

To get a practical insight about the bandpass NGD function validity of the IL shape topology, prototypes were tested via S-parameters’ measurements. The S-parameters measurements were realized by using the two-port Vector Network Analyzer (VNA) from Rohde & Schwarz® (R&D) referenced ZNB 20 and specified by frequency band 0.1 MHz to 20 GHz. The measurements were performed under the SOLT calibration by using the kit 85052D from Keysight Technologies®. Discussions on the obtained experimental results compared with calculated model and ADS® simulations will be explored in the two following subsections.

B. DISCUSSION ON “S”-IL MODELLED, SIMULATED AND EXPERIMENTAL VALIDATION RESULTS

Fig. 4 presents the experimental setup with the S-IL prototype. The performed S-parameter measurement was realized from 3.5 GHz to 3.7 GHz.

Figs. 5 display the comparisons between the calculated (“Model” plotted in dot blue curves), simulated (“ADS” plotted in dashed red curves) and measured (“Meas.” plotted in solid black curves) results of the frequency dependent GD and transmission coefficient S_{21}. Associated reflection coefficients S_{11} and S_{22} are presented in Fig. 6(a) and Fig. 6(b),

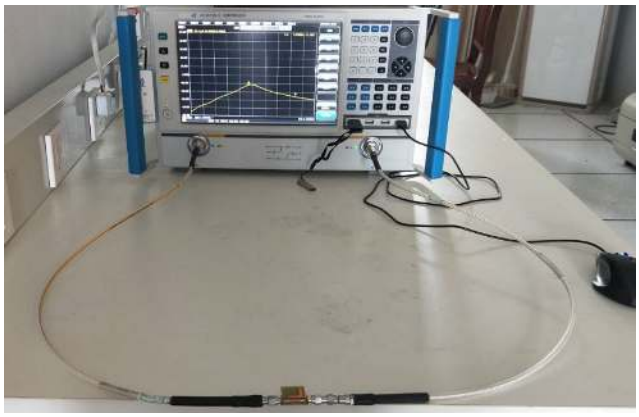

FIGURE 4. Configuration of the S-IL prototype experimental setup.

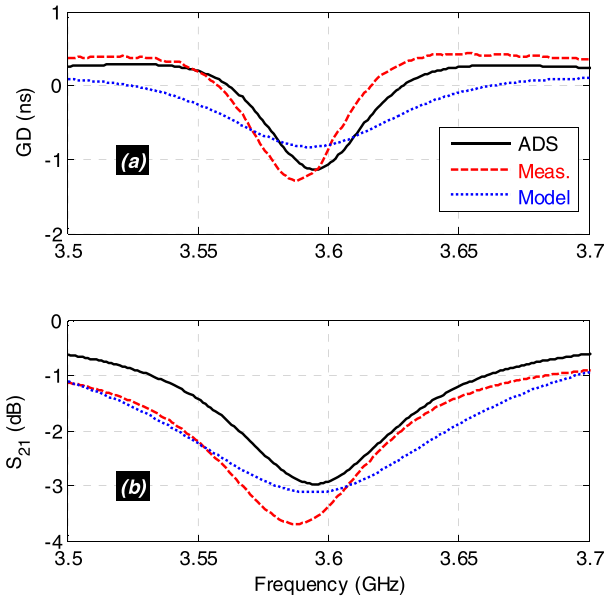

FIGURE 5. Comparisons of measured and simulated (a) GD and (b) transmission parameters from the S-IL prototype shown in Fig. 3(a).

respectively. The calculated results were computed with Matlab programming by using the S-parameters model established in formulas (23), (24) and (25). Despite the slight differences between the simulated, modelled and measured curves, the IL NGD tested circuit generates NGD of about -1 ns around the center frequency f_o of about 3.58 GHz. The slight NGD central frequency shifts between the theoretical and measurement results are mainly due to the inaccuracies of the considered dielectric substrate effective permittivity and also the metallization effects.

As expected, the results confirm that the IL NGD topology can behave as a bandpass NGD function. The NGD center frequencies, GD values, NGD bandwidth (BW) and S-parameters are summarized in Table 2. Moreover, the S IL prototype allows to achieve a very low attenuation loss better than 3 dB around the center frequency. As depicted in Fig. 6(a) and Fig. 6(b), the reflection coefficients are better than -10 dB.

TABLE 2. S-IL circuit NGD specifications.

Validation Method	f_o (GHz)	$\tau(f_o)$ (ns)	BW (MHz)	$S_{21}(f_o)$ (dB)	$S_{11}(f_o) \approx S_{22}(f_o)$ (dB)
Simu.	3.595	-1.13	67	-2.97	-12.16
Meas.	3.588	-1.29	59	-3.69	-10.72
Model	3.594	-0.83	138	-3.12	-10.18

C. DISCUSSION ON "L"-IL MODELLED, SIMULATED AND EXPERIMENTAL VALIDATION RESULTS

To complete the previous validation, the L-IL prototype was also tested. Fig. 7 sketches the configuration of the two-port VNA-based experimental setup.

Fig. 8(a) and Fig. 8(b) display the obtained results of frequency dependent GD and S_{21}, respectively. The slight offset between the calculated, simulated and measured results plotted in Figs. 8 is mainly due to the FR4 substrate characteristics. The real substrate should present higher value than given by the manufacturer and induces NGD measured center frequency lower than simulated one. Fig. 9(a) and Fig. 9(b)

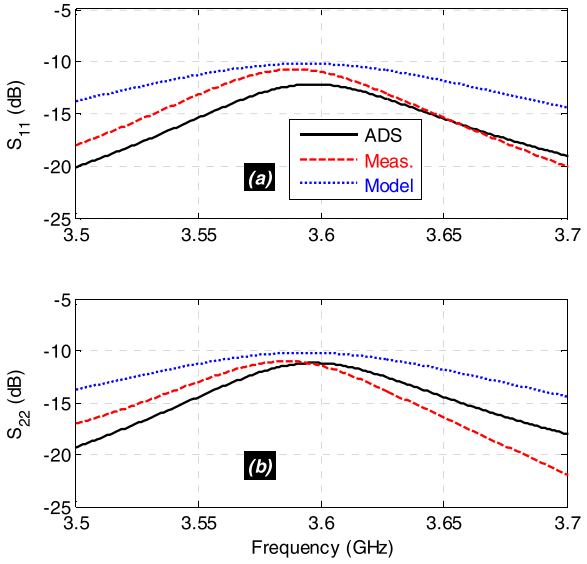

FIGURE 6. Comparisons of measured and simulated (a) S_{11} and (b) S_{22} reflection coefficients from the S-IL prototype shown in Fig. 3(a).

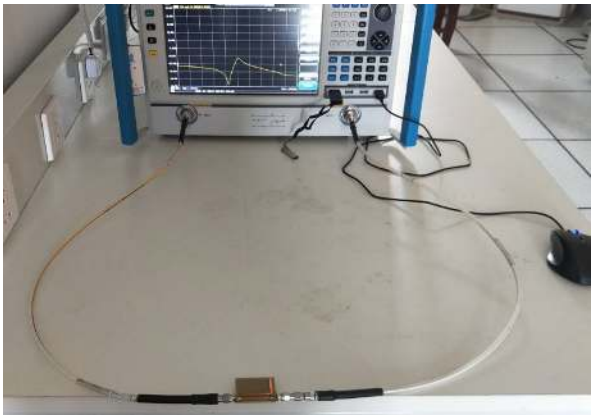

FIGURE 7. Configuration of the L-IL prototype experimental setup.

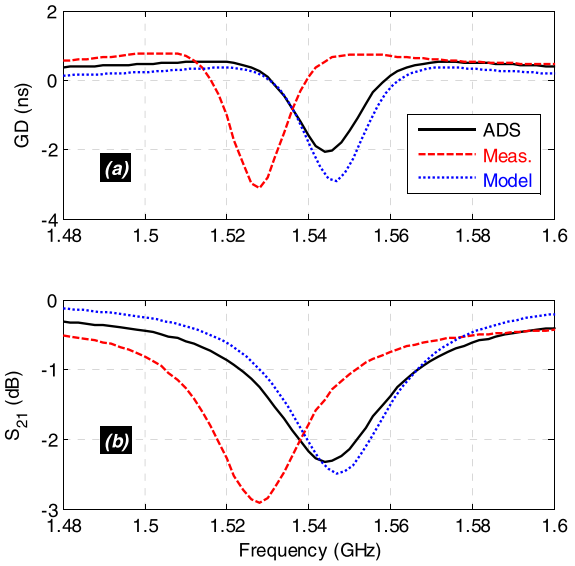

FIGURE 8. Comparisons of measured and simulated (a) GD and (b) transmission parameters from the L-IL prototype shown in Fig. 3(b).

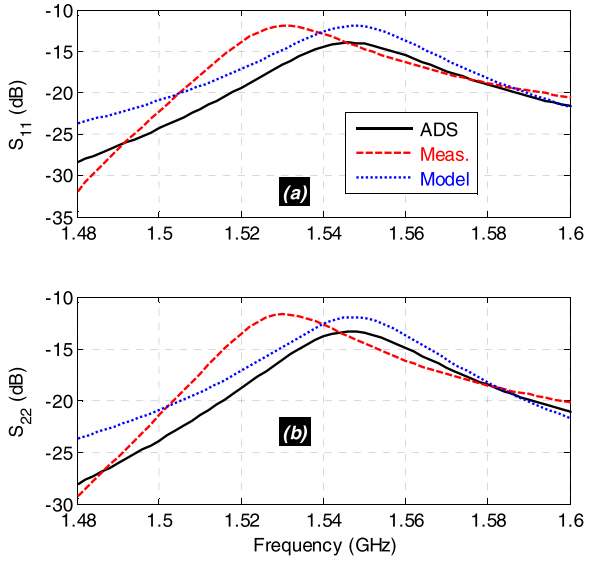

FIGURE 9. Comparisons of measured and simulated (a) S_{11} and (b) S_{22} reflection coefficients from the L-IL prototype shown in Fig. 3(b).

introduce the comparisons between the corresponding calculated, simulated and measured S_{11} and S_{22} results. Despite the slight differences between the calculated, simulated and measured results, we can point out that these comparative results are in very good agreement.

Table 3 indicates the NGD specifications of the L-IL NGD prototype. Once more, the L-IL prototype confirms the possibility to operate as an NGD bandpass function with center frequency approximately 1.544 GHz. In the NGD bandwidth, the transmission coefficient is better than −3 dB. The reflection coefficients are better than −11 dB.

D. COMPARATIVE STUDY BETWEEN NGD TOPOLOGIES

Comparisons between the NGD and S-parameter specifications of the IL NGD topology and the published ones in the literature are introduced in Table 4. It can be pointed out that the IL topology enables to operate as a bandpass NGD function with low insertion loss in addition with the good access matching. Furthermore, the topology presents significant advantages in terms of:

- Theoretical analysis,
- Design simplicity,
- To control the NGD center frequency,
- Low attenuation loss,
- Good input and output access matching,
- And the possibility to control the NGD depth.

TABLE 3. L-IL circuit NGD specifications.

Validation method	f_o (GHz)	$\tau(f_o)$ (ns)	BW (MHz)	$S_{21}(f_o)$ (dB)	$S_{11}(f_o) \approx S_{22}(f_o)$ (dB)
Simu.	1.544	-2.05	28	-2.32	-13.95
Meas.	1.528	-3.11	24	-2.91	-11.94
Model	1.547	-2.89	31	-2.49	-11.96

TABLE 4. NGD specifications comparison.

NGD Topology	f_o (GHz)	$\tau(f_o)$ (ns)	BW (MHz)	$S_{21}(f_o)$ (dB)	$S_{11}(f_o)$ (dB)
[35]	1.01	-2.09	144	-18.1	-33
[36]	2.3	-2.59	36	-4.1	-11
[37]	2.14	-6.33	70	-20.69	-29.68
[38]	1.26	-4	20	-4.3	-10
This work	1.528	-2.89	24	-2.91	-11.94

V. CONCLUSION

An innovative passive topology of IL shape geometry generating NGD function is investigated. This topology is comprised of only fully distributed elements as coupled line and open-ended lossy and delayed stub. The IL topology S-matrix from the equivalent circuit is modelled. The analytical expressions of reflection and transmission parameters is established. Then, theoretical NGD analyses are performed to determine mathematically the NGD existence condition and also the NGD specific frequencies.

The investigated IL NGD topology was validated by designing microstrip structures. The IL NGD prototypes are implemented with fully distributed elements. It was shown by the analytical calculated model, simulations and measurements that the IL NGD topology can behave as a bandpass NGD function. The simulated and measured GD and reflection, and transmission parameters are in very good agreement.

Compared to the existing NGD circuits, the IL NGD topology under study presents an advantage in terms of size reduction and flexibility to operate up to several GHz. Due to its potential integration, the developed IL NGD topology is useful for the correction of the signal delays notably in the future RF and microwave devices and systems.

REFERENCES

[1] G. Groenewold, "Noise and group delay in active filters," *IEEE Trans. Circuits Syst. I, Reg. Papers*, vol. 54, no. 7, pp. 1471–1480, Jul. 2007.

[2] S.-S. Myoung, B.-S. Kwon, Y.-H. Kim, and J.-G. Yook, "Effect of group delay in RF BPF on impulse radio systems," *IEICE Trans. Commun.*, vol. E90-B, no. 12, pp. 3514–3522, 2007.
[3] J. Rubinstein, P. Penfield, and M. A. Horowitz, "Signal delay in RC tree networks," *IEEE Trans. Comput.-Aided Design Integr. Circuits Syst.*, vol. CAD-2, no. 3, pp. 202–211, Jul. 1983.
[4] M. E. Hwang, S. O. Jung, and K. Roy, "Slope interconnect effort: Gate-interconnect interdependent delay modeling for early CMOS circuit simulation," *IEEE Trans. Circuits Syst. I, Reg. Papers*, vol. 56, no. 7, pp. 1428–1441, Jul. 2009.
[5] H. F. Li, S. C. Leung, and P. N. Lam, "Optimised synthesis of delay-insensitive circuits using time-sharing," *IEE Proc.-Comput. Digit. Techn.*, vol. 141, no. 2, pp. 111–118, Mar. 1994.
[6] E. C. Heyde, "Theoretical methodology for describing active and passive recirculating delay line systems," *Electron. Lett.*, vol. 31, no. 23, pp. 2038–2039, Nov. 1995.
[7] C. Wijenayake, Y. Xu, A. Madanayake, L. Belostotski, and L. T. Bruton, "RF analog beamforming fan filters using CMOS all-pass time delay approximations," *IEEE Trans. Circuits Syst. I, Reg. Papers*, vol. 59, no. 5, pp. 1061–1073, May 2012.
[8] S. V. Narasimhan, M. Hazarathaiah, and P. V. S. Giridhar, "Channel blind identification based on cyclostationarity and group delay," *Signal Process.*, vol. 85, no. 7, pp. 1275–1286, Jul. 2005.
[9] G. Lenz, B. J. Eggleton, C. K. Madsen, and R. E. Slusher, "Optical delay lines based on optical filters," *IEEE J. Quantum Electron.*, vol. 37, no. 4, pp. 525–532, Apr. 2001.
[10] L. Markley and G. V. Eleftheriades, "Quad-band negative-refractive-index transmission-line unit cell with reduced group delay," *Electron. Lett.*, vol. 46, no. 17, pp. 1206–1208, Aug. 2010.
[11] J. N. Munday and W. M. Robertson, "Observation of negative group delays within a coaxial photonic crystal using an impulse response method," *Opt. Commun.*, vol. 273, no. 1, pp. 32–36, 2007.
[12] L. Brillouin, *Wave Propagation and Group Velocity*. New York, NY, USA: Academic, 1960.
[13] C. G. B. Garrett and D. E. McCumber, "Propagation of a Gaussian light pulse through an anomalous dispersion medium," *Phys. Rev. A, Gen. Phys.*, vol. 1, pp. 305–313, Feb. 1970.
[14] S. Chu and S. Wong, "Linear pulse propagation in an absorbing medium," *Phys. Rev. Lett.*, vol. 48, pp. 738–741, Mar. 1982.
[15] B. Ségard and B. Macke, "Observation of negative velocity pulse propagation," *Phys. Lett. A*, vol. 109, pp. 213–216, May 1985.
[16] S. Lucyszyn, I. D. Robertson, and A. H. Aghvami, "Negative group delay synthesiser," *Electron. Lett.*, vol. 29, no. 9, pp. 798–800, Apr. 1993.
[17] C. D. Broomfield and J. K. A. Everard, "Broadband negative group delay networks for compensation of microwave oscillators and filters," *Electron. Lett.*, vol. 36, no. 23, pp. 1931–1933, Nov. 2000.
[18] G. V. Eleftheriades, O. Siddiqui, and A. K. Iyer, "Transmission line models for negative refractive index media and associated implementations without excess resonators," *IEEE Microw. Wireless Compon. Lett.*, vol. 13, no. 2, pp. 51–53, Feb. 2003.
[19] O. F. Siddiqui, M. Mojahedi, and G. V. Eleftheriades, "Periodically loaded transmission line with effective negative refractive index and negative group velocity," *IEEE Trans. Antennas Propag.*, vol. 51, no. 10, pp. 2619–2625, Oct. 2003.
[20] O. F. Siddiqui, S. J. Erickson, G. V. Eleftheriades, and M. Mojahedi, "Time-domain measurement of negative group delay in negative-refractive-index transmission-line metamaterials," *IEEE Trans. Microw. Theory Techn.*, vol. 52, no. 5, pp. 1449–1454, May 2004.
[21] K.-P. Ahn, R. Ishikawa, A. Saitou, and K. Honjo, "Synthesis for negative group delay circuits using distributed and second-order RC circuit configurations," *IEICE Trans. Electron.*, vol. E92-C, no. 9, pp. 1176–1181, 2009.
[22] B. Ravelo, "Investigation on microwave negative group delay circuit," *Electromagnetics*, vol. 31, no. 8, pp. 537–549, Nov. 2011.
[23] S. Park, H. Choi, and Y. Jeong, "Microwave group delay time adjuster using parallel resonator," *IEEE Microw. Wireless Compon. Lett.*, vol. 17, no. 2, pp. 109–111, Feb. 2007.
[24] K.-J. Song, S.-G. Kim, H.-J. Choi, and Y.-C. Jeong, "Group delay time matched CMOS microwave frequency doubler," *J. Korean Inst. Electromagn. Eng. Sci.*, vol. 19, no. 7, pp. 771–777, 2008.
[25] K.-P. Ahn, R. Ishikawa, and K. Honjo, "Group delay equalized UWB InGaP/GaAs HBT MMIC amplifier using negative group delay circuits," *IEEE Trans. Microw. Theory Techn.*, vol. 57, no. 9, pp. 2139–2147, Sep. 2009.
[26] H. Choi, Y. Jeong, C. D. Kim, and J. S. Kenney, "Efficiency enhancement of feedforward amplifiers by employing a negative group-delay circuit," *IEEE Trans. Microw. Theory Techn.*, vol. 58, no. 5, pp. 1116–1125, May 2010.
[27] M. Kandic and G. E. Bridges, "Bilateral gain-compensated negative group delay circuit," *IEEE Microw. Compon. Lett.*, vol. 21, no. 6, pp. 308–310, Jun. 2011.
[28] B. Ravelo, "Distributed NGD active circuit for RF-microwave communication," *AEU-Int. J. Electron. Commun.*, vol. 68, no. 4, pp. 282–290, Apr. 2014.
[29] H. Mirzaei and G. V. Eleftheriades, "Realizing non-Foster reactive elements using negative-group-delay networks," *IEEE Trans. Microw. Theory Techn.*, vol. 61, no. 12, pp. 4322–4332, Dec. 2013.
[30] T. Zhang, R. Xu, and C.-T. M. Wu, "Unconditionally stable non-foster element using active transversal-filter-based negative group delay circuit," *IEEE Microw. Wireless Compon. Lett.*, vol. 27, no. 10, pp. 921–923, Oct. 2017.
[31] H. Mirzaei and G. V. Eleftheriades, "Arbitrary-angle squint-free beamforming in series-fed antenna arrays using non-foster elements synthesized by negative-group-delay networks," *IEEE Trans. Antennas Propag.*, vol. 63, no. 5, pp. 1997–2010, May 2015.
[32] L. He, W. Li, J. Hu, and Y. Xu, "A 24-GHz source-degenerated tunable delay shifter with negative group delay compensation," *IEEE Microw. Wireless Compon. Lett.*, vol. 28, no. 8, pp. 687–689, Aug. 2018.
[33] Y. Meng, Z. Wang, S. Fang, T. Shao, and H. Liu, "A broadband switchless bi-directional amplifier with negative-group-delay matching circuits," *Electronics*, vol. 7, no. 9, p. 158, Aug. 2018.
[34] M. Kandic and G. E. Bridges, "Asymptotic limits of negative group delay in active resonator-based distributed circuits," *IEEE Trans. Circuits Syst. I, Reg. Papers*, vol. 58, no. 8, pp. 1727–1735, Aug. 2011.
[35] Z. Wang, Y. Cao, T. Shao, S. Fang, and Y. Liu, "A negative group delay microwave circuit based on signal interference techniques," *IEEE Microw. Wireless Compon. Lett.*, vol. 28, no. 4, pp. 290–292, Apr. 2018.
[36] F. Wan, N. Li, B. Ravelo, Q. Ji, and J. Ge, "S-parameter model of three parallel interconnect lines generating negative group-delay effect," *IEEE Access*, vol. 6, pp. 57152–57159, 2018.
[37] G. Chaudhary and Y. Jeong, "Transmission-type negative group delay networks using coupled line doublet structure," *IET Microw., Antennas Propag.*, vol. 9, no. 8, pp. 748–754, Jun. 2015.
[38] B. Ravelo, "Theory of coupled line coupler-based negative group delay microwave circuit," *IEEE Trans. Microw. Theory Techn.*, vol. 64, no. 11, pp. 3604–3611, Nov. 2016.
[39] R. Das, Q. Zhang, and H. Liu, "Lossy coupling matrix synthesis approach for the realization of negative group delay response," *IEEE Access*, vol. 6, pp. 1916–1926, 2018.

BLAISE RAVELO received the Ph.D. degree from the University of Brest, in 2008, and his dissertation led to research Habilitation à Diriger des Recherches (HDR) from the University of Rouen, in 2012. He is currently a Full Professor with the Nanjing University of Information Science and Technology. He is a pioneer of the negative group delay (NGD) RF/analog and digital circuits, and systems. He is coauthor of more than 200 articles and regularly involved in national/international research projects. He co-supervised and directed nine Ph.D. students and six Ph.D. candidates who defended. He participates regularly in large Research and Development international projects. His current publication H-index is 16 (Reference: Google Scholar 2017). His research interests include microwave circuit design, electromagnetic compatibility (EMC) and interference (EMI), and signal and power integrity (SI/PI) engineering.

Dr. Ravelo is the Scientific Chair of the 5th International Conference on Electromagnetic Near Field Characterization and Imaging, in 2011, a member of Advanced Electromagnetic Symposium 2013-2018 technical committee and a member of the IEEE RADIO 2015 scientific committee. He has been a URSI member and regularly invited to review articles submitted to international journals (the IEEE TMTT, IEEE Access, IEEE TCS, IEEE TEMC, IEEE TIM, IEEE TIE, *Journal of Electromagnetic Waves and Applications*, IET CDS, IET MAP, and *International Journal of Electronics*, and so on.) and international books (Wiley, Intech Science, and so on.).

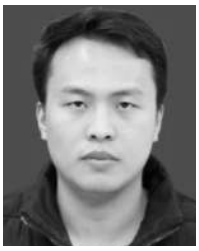

NINGDONG LI received the B.Sc. degree in electrical engineering from Anhui Polytechnic University, Wuhu, China, in 2017. He is currently pursuing the M.S. degree with the Nanjing University of Information Science and Technology, Nanjing, China. His research interests include abnormal wave propagation in dispersive media and microwave circuits.

FAYU WAN received the Ph.D. degree in electronic engineering from the University of Rouen, Rouen, France, in 2011. From 2011 to 2013, he was a Postdoctoral Fellow with the Electromagnetic Compatibility Laboratory, Missouri University of Science and Technology, Rolla. He is currently a Full Professor with the Nanjing University of Information Science and Technology, Nanjing, China. His current research interests include negative group delay circuits, electrostatic discharge, electro-magnetic compatibility, and advanced RF measurement.

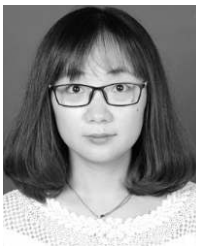

JIAO FENG received the Ph.D. degree in wireless communications from Southampton University, U.K., in 2014, and the B.Eng. and M.Sc. degrees in communications engineering from Jilin University, Jilin, China, in 2007 and 2009, respectively. Since 2014, she has been with the School of Electric and Information Engineering, Nanjing University of Information Science and Technology, China. She is involved in the projects sponsored by the National Natural Science Foundation and by the Natural Science Foundation of Jiangsu Province. Her research interests include cooperative communication, network protocols, digital signal processing, cognitive radio networks, matching theory, machine learning, and natural language processing.